J. Fluid Mech., page 1 of 25. © Cambridge University Press 2011
doi:10.1017/jfm.2011.489

Simulation of a propelled wake with moderate excess momentum in a stratified fluid

Matthew B. de Stadler and Sutanu Sarkar†

Department of Mechanical and Aerospace Engineering, University of California San Diego, La Jolla, CA 92093, USA

(Received 17 April 2011; revised 16 August 2011; accepted 3 November 2011)

Direct numerical simulation is used to simulate the turbulent wake behind an accelerating axisymmetric self-propelled body in a stratified fluid. Acceleration is modelled by adding a velocity profile corresponding to net thrust to a self-propelled velocity profile resulting in a wake with excess momentum. The effect of a small to moderate amount of excess momentum on the initially momentumless self-propelled wake is investigated to evaluate if the addition of excess momentum leads to a large qualitative change in wake dynamics. Both the amount and shape of excess momentum are varied. Increasing the amount of excess momentum and/or decreasing the radial extent of excess momentum was found to increase the defect velocity, mean kinetic energy, shear in the velocity gradient and the wake width. The increased shear in the mean profile resulted in increased production of turbulent kinetic energy leading to an increase in turbulent kinetic energy and its dissipation. Slightly larger vorticity structures were observed in the late wake with excess momentum although the differences between vorticity structures in the self-propelled and 40 % excess momentum cases was significantly smaller than suggested by previous experiments. Buoyancy was found to preserve the doubly inflected velocity profile in the vertical direction, and similarity for the mean velocity and turbulent kinetic energy was found to occur in both horizontal and vertical directions. While quantitative differences were observed between cases with and without excess momentum, qualitatively similar evolution was found to occur.

Key words: stratified turbulence, wakes

1. Introduction

The near wake behind a propelled body is fundamentally different from its towed counterpart. As shown in figure 1, a towed wake contains only a velocity deficit in the wake whereas a propelled wake contains velocity excess and deficit resulting in a doubly inflected mean velocity profile. Figure 1(*b*) illustrates the special case where the momentum in the drag lobes balances the momentum in the thrust lobe resulting in a momentumless wake; such a profile is characteristic of a self-propelled body moving at constant speed. Figure 1(*c*) shows an example of a self-propelled body undergoing acceleration. The velocity profile in figure 1(*b*) was observed experimentally for the mean velocity in the near wake by Naudascher (1965), Aleksenko & Kostomakha

† Email address for correspondence: ssarkar@ucsd.edu

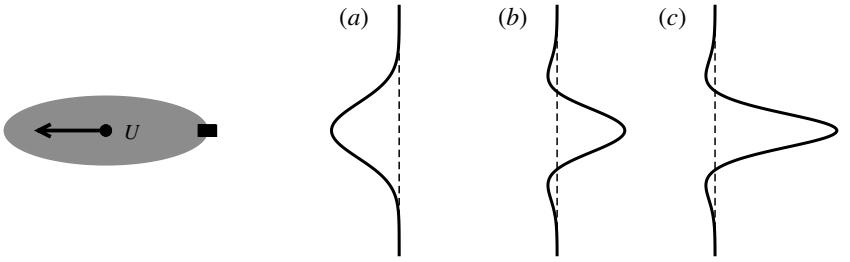

FIGURE 1. Velocity profiles in the wake of towed and jet-propelled bodies. This image shows the fluid velocity behind the moving body shown on the left. (*a*) Dragged body with no propulsion. (*b*) Self-propelled body with zero net momentum. (*c*) Propelled body with excess momentum. The dashed line corresponds to zero velocity.

(1987), Higuchi & Kubota (1990) and Sirviente & Patel (2000*a*) in unstratified non-swirling axial jet-propelled momentumless wake studies, and for an unstratified swirling axial jet-propelled momentumless wake by Kostomakha & Lesnova (1995). The mirror image of figure 1(*b*) was obtained in momentumless cases with a propeller by Hyun & Patel (1991*a*,*b*) and Sirviente & Patel (2000*b*) for an off-centre swirling jet. It is important to note that in the presence of stratification, an initially momentumless wake will acquire a net momentum during its evolution due to the transfer of momentum from the wake to the background by internal waves. In addition, stratification is known to significantly alter the mean velocity profile during the downstream evolution. In contrast to the coherent profile observed in unstratified experiments, Meunier & Spedding (2006) observed no coherent mean velocity profile in the intermediate and late wake in their experiments with a momentumless self-propelled body in a stratified fluid.

Experimentally, stratified wakes are usually studied by towing a body, often a sphere, or by towing a body with an independent momentum source, generating what we refer to as a propelled wake, which can balance the momentum deficit in the wake to create a momentumless wake. Note that it is extremely challenging, if not impossible, to obtain a truly momentumless wake; in practice experiments have a momentum imbalance on the order of 1 % (Novikov 2009). Only recently have remote-controlled submersibles been used to represent a true self-propelled wake, e.g. Voropayev *et al.* (2007) and Voropayev & Fernando (2010).

For a propelled wake, the momentum source can take a number of forms including propellers, swirling jets, and non-swirling jets. Numerous experimental studies, mostly with an unstratified background, have shown that the wake behaves differently depending on the momentum source for a momentumless wake, see for example Schetz & Jakubowski (1975), Park & Cimbala (1991) and Sirviente & Patel (2000*b*, 2001). The presence of swirl is known to result in significant differences in both the net-momentum and momentumless cases; the effect is especially strong in the momentumless cases as noted by Chernykh, Demenkov & Kostomakha (2005) in their review of relevant literature. Further detail on the effect of swirl is summarized in the review of Schetz (1980) and the literature review on wakes in § 5.7 of Piquet (1999). Results from unstratified wind tunnel experiments on propelled bodies with net momentum, such as the three-dimensional study by Higuchi & Kubota (1990) and the two-dimensional study of Cimbala & Park (1990), are not generally expected to extend to the case of a stratified wake as stratification significantly affects the wake dynamics.

The following paragraphs discuss work related to the wake of axisymmetric propelled bodies.

Wakes of self-propelled bodies were first discussed by Schooley & Stewart (1963), and remained an area of intense interest until the early 1980s when research efforts emphasized the wake behind spheres. A partial summary of results from early self-propelled wake studies in a stratified fluid can be found in the review article Lin & Pao (1979). After a long hiatus, self-propelled wakes were investigated recently in laboratory experiments that employed modern diagnostics by Meunier & Spedding (2006). Voropayev *et al.* (1999) and Voropayev & Fernando (2010) also investigated self-propelled wakes, although their studies emphasized the effect of acceleration manoeuvres on the formation of large eddies in the late wake of a self-propelled body. Direct numerical simulation (DNS) was used by Brucker & Sarkar (2010) to compare self-propelled and towed wakes at a Reynolds number of 50 000.

There is strong evidence from unstratified experimental studies that a self-propelled wake is qualitatively different from a towed wake; the mean velocity and streamwise turbulence intensity decay faster (Higuchi & Kubota 1990) and the mean shear is significantly reduced in the self-propelled profile (Sirviente & Patel 2000*a*). In a stratified fluid, Lin & Pao (1979) observed a more complicated late-wake vorticity field with smaller horizontal scales and spacings compared to a towed wake. Smaller horizontal scales and spacing between vortices of a self-propelled wake relative to a towed wake was also observed by Meunier & Spedding (2006) and Brucker & Sarkar (2010). Brucker & Sarkar (2010) found that the mean velocity decayed significantly faster in a self-propelled wake relative to a towed wake; this result is consistent with unstratified experiments. However, Meunier & Spedding (2006) found that the quadratic horizontal velocity fluctuations decayed slower in a self-propelled wake relative to a towed wake; this result is in contrast to the results observed for the integrated turbulent kinetic energy given in Brucker & Sarkar (2010).

While a number of differences are known to occur between a canonical towed wake and a self-propelled wake, far less attention has been devoted to the case of a propelled wake with a small to intermediate amount of excess momentum. Analytical studies are limited to the similarity analysis of Tennekes & Lumley (1972) and a solution using a linearized interferential model of wake development by Novikov (2009), both of which are for wakes in an unstratified fluid. Higuchi & Kubota (1990) considered the case of a propelled wake with moderate excess momentum in an unstratified fluid and Meunier & Spedding (2006) considered the case of a propelled wake with a small amount of excess momentum in a stratified fluid. Numerical work for the unstratified case was performed using a Reynolds-averaged Navier–Stokes (RANS) model by Lewellen, Teske & Donaldson (1974) and Chernykh, Moshkin & Fomina (2009) and with DNS by de Stadler & Sarkar (2011*a*) in a companion study to the present one. The only numerical work on the stratified case has been done using RANS by Chernykh *et al.* (2009).

Tennekes & Lumley (1972) consider what happens when a momentumless self-propelled wake is contaminated by a small amount of excess momentum in an unstratified fluid. Based on a self-similarity analysis they determine that the defect velocity of the excess momentum component decays as $U_0 \propto x^{-2/3}$, where U_0 is the defect velocity and x is the downstream distance, and the defect velocity of the self-propelled component decays as $U_0 \propto x^{-4/3}$. Thus, they deduce that a self-propelled wake with even a small amount of excess momentum differs significantly from a self-propelled wake without excess momentum where $U_0 \propto x^{-4/5}$. However, this result requires the usage of two unverified assumptions: that the turbulent viscosity is

constant across the wake; and that the velocity can be treated as a superposition of two independently varying components, a momentumless one and a Gaussian excess momentum component.

In experiments using towed cylinders and streamlined bodies with a thrust-producing propeller, Meunier & Spedding (2006) found that a propelled wake with momentum as small as 2 %, behaves qualitatively differently than a momentumless wake and can be scaled as a momentum wake with appropriate normalization by an effective momentum thickness. Note that this conclusion is based on statistics taken on a horizontal plane at the vertical centreline. Meunier & Spedding (2006) also found that a momentumless propelled wake at a small angle of attack generates a three-lobed vorticity structure and the velocity becomes self-similar, retaining the initially asymmetric profile. The asymmetric momentumless case introduced in Meunier & Spedding (2006) is discussed in detail by Gallet, Meunier & Spedding (2006) who found that both the wake width and maximum velocity decayed at the same rate as a momentum wake when the velocity is normalized appropriately. As a result of their observation that the wake is strongly sensitive to small amounts of excess momentum as well as the angle of attack of the body, Meunier & Spedding (2006) question whether a momentumless wake ever exists in practice.

Voropayev *et al.* (1999) observed the formation of significantly larger eddy structures in the late wake of an accelerating body compared to a self-propelled body at low Reynolds number, $Re \approx 630$, in a stratified fluid. They used a towed model submarine with a thrust-producing axial jet to control the amount of acceleration. In a follow up study, Voropayev & Fernando (2010) used a remote-controlled propeller-driven submarine to conduct similar experiments at higher Reynolds number, $Re = O(10\,000)$, and Froude number, $Fr \approx 1$, and with different levels of acceleration. Although data for a weak acceleration are not shown, Voropayev & Fernando (2010) state that the results for that case are similar to the case discussed where a vorticity front is formed upon acceleration with the fluid behind the front moving faster than the front leading to the later fluid becoming entrained into the front region forming a large dipole.

Numerical work for the case of a stratified, self-propelled wake with excess momentum is limited to Chernykh *et al.* (2009), who employ a modified k–ε turbulence model for their RANS simulations. Chernykh *et al.* (2009) found that a small amount of excess momentum has a significant effect on the defect velocity but a small impact on turbulent kinetic energy and internal wave radiation. Note that their solution technique used symmetry arguments to solve the flow in one quadrant of the domain. While de Stadler & Sarkar (2011*a*) observed quantitative differences in statistics for cases with differing amounts and shapes of excess momentum in an unstratified fluid, there was little qualitative difference between cases with the exception of the mean kinetic energy where the cases with increased amounts of excess momentum diverged earlier from momentumless behaviour.

Brucker & Sarkar (2010) performed DNS of initially momentumless wakes and found that they decay faster than towed wakes. Larger shear production of turbulence for the momentumless wake profile was identified as the reason for more rapid decay. The buoyancy-induced reduction of vertical Reynolds shear stress was found to decrease mean-to-turbulence transfer and allow the wake to be long-lived in a stratified fluid compared to an unstratified fluid. They also found that the standard regimes for towed wake evolution, i.e. near-wake (NW), non-equilibrium (NEQ) and quasi-two-dimensional (Q2D) regimes, occurred in self-propelled wakes as well, with the NEQ regime being prolonged at higher Reynolds number. The longer duration of

the NEQ regime was predicted analytically based on a model for a momentum wake in a stratified fluid by Meunier, Diamessis & Spedding (2006) and was observed in the numerical simulations of a momentum wake by Diamessis, Spedding & Domaradzki (2011).

1.1. *Objectives*

The present study is designed to investigate the effect of excess momentum on the downstream evolution and wake structure of an initially momentumless wake in a stratified fluid. Numerical simulation is employed for this study as it allows precise control over the location, shape, and extent of excess momentum. Fully three-dimensional simulations are performed using DNS to study the effect of excess momentum from the near wake to the far wake; note that the present simulations are the first usage of DNS for this problem. Here we present quantitative and qualitative data describing the self-propelled wake dynamics in the presence of varying amounts and shapes of excess momentum. The most common application for the present study is the wake of a self-propelled submersible moving in the littoral region of the ocean.

Qualitative questions of interest for the present study include: (i) How does the amount of excess momentum affect the downstream development of the wake? (ii) How does the shape of excess momentum affect the downstream development of the wake? (iii) How does excess momentum affect the size of late-wake eddies? (iv) What features of the initial flow structure, if any, are preserved in the late wake? We also quantify the effect of excess momentum on characteristic wake scales and wake energetics. Vertical profiles of mean and turbulence quantities have not been reported previously and are characterized here. Results for cases with excess momentum are compared with an initially momentumless self-propelled wake as well as the experimental data of Meunier & Spedding (2006) for propelled wakes and the limiting cases of self-propelled and towed bodies.

2. Formulation

The formulation for this paper is similar to that used by Brucker & Sarkar (2010) and de Stadler, Sarkar & Brucker (2010). The description given here emphasizes differences between the present study and these two.

For this study we consider the wake behind a self-propelled body of effective diameter D moving at speed U in a fluid with a linear density stratification. The body is initially moving at constant speed such that the thrust and drag balance in the near wake resulting in zero net momentum. Suddenly the body accelerates, transferring net momentum into the wake over a finite time interval. This accelerating manoeuvre is modelled as excess momentum being applied to the initially momentumless wake profile. Physically, this problem setup corresponds to an overthrusted wake which is being towed at constant speed while employing an independent propulsor to generate thrust in excess of the drag. Such a situation has been considered experimentally by Higuchi & Kubota (1990) in an unstratified fluid and Meunier & Spedding (2006) in a stratified fluid.

Ideally, we would like to perform these simulations with the body inside the computational domain in a frame similar to a wind tunnel where fluid flows past the body. This is not possible due to the prohibitive computational cost of resolving the fine scales occurring close to the body. Even without resolving the body in the domain, it is extremely expensive to perform a spatially evolving simulation as domain sizes on the order of thousands of body diameters downstream are of interest and the

large vortex structures that form in the late wake require substantial domain size in the horizontal direction as well. Owing to the high computational cost of performing such a simulation in a spatially evolving frame, the temporal approximation is used to simulate the problem in a temporal frame following previous authors, see Brucker & Sarkar (2010) for a list of stratified and unstratified simulations using the temporal approximation. A limitation of the present study, due to the temporal approximation, is that information is not allowed to travel downstream as would be the case in a spatially evolving wake where the excess momentum would interact with the initially momentumless wake further downstream.

The temporal frame moves with a velocity of U in the positive streamwise direction which corresponds to the wake evolving behind a body moving with velocity U in the negative streamwise direction. Note that in this formulation, the x_1 direction is periodic. Statistics in the temporal frame are related to those in the spatial frame by the relation $x = x_0 + Ut$ where x is the distance behind the body in the streamwise direction, x_0 is the spatial location corresponding to the initial conditions for the temporal simulation, and t is the time evolved in the temporal simulation.

The three-dimensional, incompressible, unsteady form of the Navier–Stokes equations subject to the Boussinesq approximation are the governing equations for this problem. DNS is used to advance the solution from the near wake to the far wake. All relevant scales of motion are resolved and no turbulence models are used. The numerical scheme employed is identical to that given in Brucker & Sarkar (2010), see that reference for details.

2.1. *Boundary conditions*

Boundary conditions for this study are taken to correspond to an undisturbed background with a linear density stratification. Stress-free boundary conditions are applied at the x_2–x_3 boundaries for the velocity terms. The vertical density gradient is maintained at the value corresponding to the background at the x_3 boundary. At the x_2 boundary $\partial\rho/\partial x_2 = 0$ is enforced. By definition, all flow variables are periodic in the x_1 direction in the temporal approximation. As in de Stadler *et al.* (2010) a sponge region is employed over 20 gridpoints at both the x_2 and x_3 boundaries to avoid spurious reflections from waves and other disturbances that propagate out of the computational domain; the details of the sponge region are identical to those given in de Stadler *et al.* (2010).

2.2. *Initial conditions*

As the self-propelled wake is notoriously sensitive to initial conditions as noted by Meunier & Spedding (2006), we initialize our simulations with the idealized doubly inflected mean velocity profile of Rottman *et al.* (2003), which was also used by Brucker & Sarkar (2010), that is representative of the near wake of a body moving under its own power. The opening paragraph of this paper contains a list of experiments with qualitatively similar velocity profiles to that used in the present study. Detailed experimental data describing the near wake of a self-propelled body are not available for the Reynolds numbers under consideration, for a stratified or unstratified fluid, so the initial conditions of Brucker & Sarkar (2010) were used as a guide for both the mean and fluctuating components of the velocity field.

2.2.1. *Initial condition generation procedure*

All simulations began with an initially momentumless self-propelled wake profile. Note that the designation *SP* will be used to refer to the case with zero net

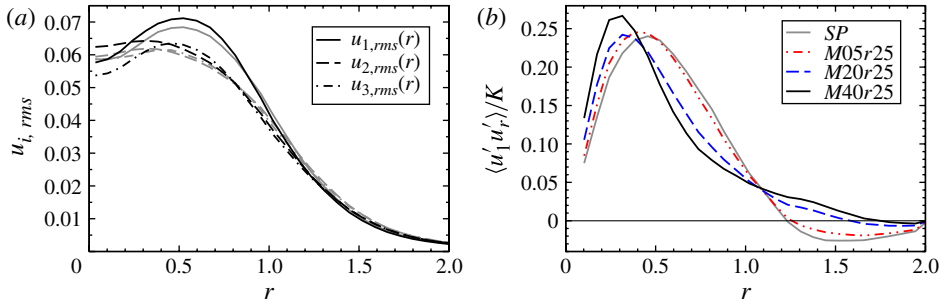

FIGURE 2. (Colour online available at journals.cambridge.org/flm) Initial conditions at the end of the initialization procedure for the $r_M = 0.25$ cases. (*a*) Velocity r.m.s. components; grey lines are used for *SP* and black lines for *M*40*r*25. Cases *M*20*r*25 and *M*05*r*25 are in between the *SP* and *M*40*r*25 cases. (*b*) $\langle u_1' u_r' \rangle / K$. See table 1 for parameters for each of the simulations.

momentum in the wake. The *SP* case was initialized as described by Brucker & Sarkar (2010). Excess momentum was added as described later in § 2.2.2. No swirl is present in the initial conditions. The initial mean velocity field is constructed as $U_1(r) = u_{SP}(r) + \delta u(r)$, with u_{SP} and δu given by

$$u_{SP}(r) = U_0 \left[1 - \frac{1}{2} \left(\frac{r}{r_0} \right)^2 \right] \exp[-(1/2)\,(r/r_0)^2], \tag{2.1a}$$

$$\delta u(r) = U_0 c_M\,(r_0/r_M)^2 \exp[-(1/2)\,(r/r_M)^2], \tag{2.1b}$$

where $r_0 = 0.5$, $U_0 = 0.11$, $\delta u(r)$ is the excess momentum profile, c_M controls the amount of excess momentum, and r_M controls the shape of the excess momentum. Turbulent fluctuations with a given spectrum are superposed on $U_1(r)$ and then spatially limited following Brucker & Sarkar (2010). The spectrum used is

$$E(k) = \left(\frac{k}{k_0} \right)^4 \exp[-2\,(k/k_0)^2] \tag{2.2}$$

where $k_0 = 4$. The fluctuations are cropped to the wake region using the limiting function $g(r)$,

$$g(r) = a \left(1 + \frac{r^2}{r_0^2} \right) \exp[-(1/2)\,(r/r_0)^2] \tag{2.3}$$

where $a = 0.055$ is the maximum initial centreline amplitude of the velocity fluctuations.

The initial velocity field is allowed to adjust following the unstratified Navier–Stokes equations until $\max(\langle u_1' u_r' \rangle / K) \approx 0.25$; here angle brackets indicate a streamwise average and $K = \langle u_i' u_i' \rangle / 2$ is the turbulent kinetic energy. During this time, the mean velocity field is held constant and the fluctuations adjust to the mean profile. The initial velocity fluctuation fields at the start of the simulation are shown in figure 2.

2.2.2. *Adding excess momentum*

As a first attempt to study this problem, an accelerating manoeuvre was approximated by adding a velocity profile corresponding to net thrust to a self-propelled velocity profile resulting in a wake with excess momentum. There are a

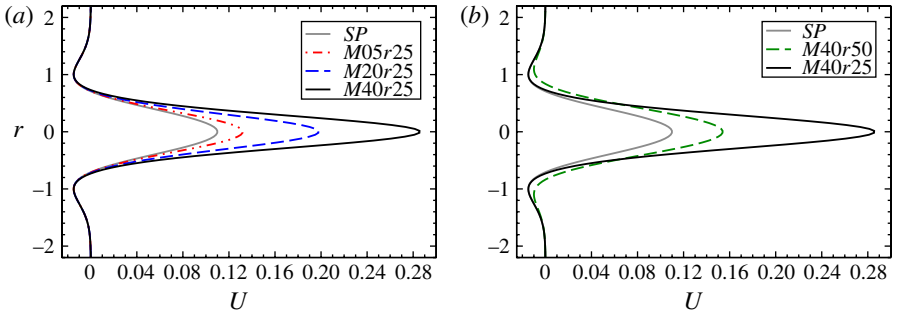

FIGURE 3. (Colour online) Initial mean profiles. (*a*) $r_M = 0.25$: three different values of excess momentum are imposed by changing c_M. (*b*) $c_M = 0.4$: two different shapes are imposed on the excess momentum by varying r_M.

number of shapes that can be used for the excess momentum. For this study, the excess momentum is applied as a Gaussian profile, equation (2.1), with a parameter to control the shape of the excess momentum, r_M, and a parameter to control the amount of excess momentum, c_M. Applying excess momentum in this manner corresponds to superposing a developed jet that began with a radial top-hat velocity profile at the body onto the initially momentumless velocity profile. The effect of varying the shape and amount of excess momentum is shown in figure 3.

One also has freedom to choose a reference value of momentum for calculating the amount of excess momentum injected. For this work, the reference value was chosen to be the amount of momentum in the Gaussian term of U_{SP}, $U_0 \exp(-(1/2)\,(r/r_0)^2)$ in (2.1); this definition is equivalent to that of Higuchi & Kubota (1990). Thus, $c_M = 0.4$ corresponds to 40 % excess momentum using our definition.

2.3. *Simulation parameters*

Numerical simulations were designed to study the effect of excess momentum on the wake by varying two parameters: the radial extent of the excess momentum and the strength of the excess momentum. Two values were chosen for the radial extent r_M: one equal to the radial extent of the mean profile to allow comparison with the mixed wake of Tennekes & Lumley (1972); and one with a narrower radial extent to represent an axial jet used to propel a body. The amount of excess momentum c_M was chosen to represent the effect of a small to moderate change in velocity. Three values were used to study the influence of successively increasing the acceleration. Our computational resources, combined with data from Brucker (2009), made a Reynolds number of 10 000 an attractive choice. Simulations were designed for a resolution of $\Delta x/\eta \leqslant 4$, where Δx is the smallest grid spacing and η is the Kolmogorov length scale. Each case required approximately 1650 CPU hours on Einstein, a Cray XT5. All the simulation parameters are listed in table 1.

3. Data analysis methods

One of the advantages of numerical simulations is that they produce full three-dimensional fields for all flow variables. This allows direct measurement of quantities inaccessible to experimentalists such as turbulent dissipation. To analyse these data, streamwise averages, area-integrated quantities and contour plots are used. The Reynolds decomposition is used to write variables as the combination of a mean and

Case	$100 \times c_M$	r_M	Re	Fr	Pr	L_1	L_2	L_3	n_1	n_2	n_3	t_f
SP	0	n/a	10 000	3	1	48.125	24.883	11.758	1408	768	384	2276
*M*05*r*25	5	0.25	10 000	3	1	48.125	24.883	11.758	1408	768	384	2267
*M*20*r*25	20	0.25	10 000	3	1	48.125	24.883	11.758	1408	768	384	2026
*M*40*r*25	40	0.25	10 000	3	1	48.125	24.883	11.758	1408	768	384	1495
*M*05*r*50	5	0.50	10 000	3	1	48.125	24.883	11.758	1408	768	384	2254
*M*20*r*50	20	0.50	10 000	3	1	48.125	24.883	11.758	1408	768	384	2067
*M*40*r*50	40	0.50	10 000	3	1	48.125	24.883	11.758	1408	768	384	1951

TABLE 1. Simulation parameters. In the labelling of the cases, *SP* denoted self-propelled; the number following *M* refers to the strength of the excess momentum c_M, and the number following *r* refers to its radial extent r_M. L_i refers to the size of the computational domain in a given direction (not including the sponge region), n_i refers to the number of gridpoints in a given direction and t_f refers to the end time of the simulation.

a fluctuating component, $\phi(x_1, x_2, x_3, t) = \langle\phi\rangle(x_2, x_3, t) + \phi'(x_1, x_2, x_3, t)$, where angle brackets indicate a streamwise average. In the following sections, figures showing data as a function of time also show the time evolved in buoyancy timescales Nt, where N is the buoyancy frequency, on the top horizontal axis.

We are interested in measuring characteristic velocity and length scales for the wake. The defect velocity is defined as the maximum value of the streamwise velocity in the temporal frame. The wake dimensions are defined following Brucker & Sarkar (2010):

$$R_\alpha^2(t) = F\frac{\displaystyle\int_A \left(x_\alpha - x_\alpha^c\right)^2 \langle u_1\rangle^2 \,\mathrm{d}A}{\displaystyle\int_A \langle u_1\rangle^2 \,\mathrm{d}A}, \quad x_\alpha^c(t) = \frac{\displaystyle\int_A x_\alpha \langle u_1\rangle^2 \,\mathrm{d}A}{\displaystyle\int_A \langle u_1\rangle^2 \,\mathrm{d}A}, \tag{3.1}$$

where $F = 2$ is a normalization factor to set the initial wake width, R_2, and height, R_3, to 0.5 in the case with zero net momentum, and A is the area of the x_2–x_3 plane not including the sponge region. One can also define similar length scales for the turbulent kinetic energy, R_{K2} and R_{K3}, and the kinetic energy R_{E2} and R_{E3}, by replacing $\langle u_1^2\rangle$ with $K = \langle u_i' u_i'\rangle/2$ or $E = (\langle u_i\rangle\langle u_i\rangle + \langle u_i' u_i'\rangle)/2$ in (3.1). Note that due to the method of defining the wake dimensions, a wake with excess momentum will have a larger velocity weighting closer to the origin which results in the denominator increasing more than the numerator so by definition the initial wake dimensions will be reduced.

We are also interested in measuring the energy associated with the wake. The integrated mean kinetic energy, MKE, and integrated turbulent kinetic energy, TKE, are defined as

$$\mathrm{MKE} = \int_A \frac{1}{2}\langle u_i\rangle\langle u_i\rangle \,\mathrm{d}A, \quad \mathrm{TKE} = \int_A \frac{1}{2}\langle u_i' u_i'\rangle \,\mathrm{d}A. \tag{3.2}$$

In addition to the integrated turbulent kinetic energy, we are also interested in measuring the energy budget of the turbulent kinetic energy, $K = \langle u_i' u_i'\rangle/2$. The evolution equation for the turbulent kinetic energy is given as

$$\frac{\mathrm{D}K}{\mathrm{D}t} = P + B - \varepsilon - \frac{\partial T_i}{\partial x_i} \tag{3.3}$$

where production, P, dissipation, ε, buoyancy flux, B, and turbulent transport, $\partial T_i/\partial x_i$, are given by the standard definitions, see (Pope 2000) for details:

$$P = -\langle u_i' u_j' \rangle \frac{\partial \langle u_i \rangle}{\partial x_j}, \quad \varepsilon = \frac{1}{Re} \left\langle \frac{\partial u_i'}{\partial x_k} \frac{\partial u_i'}{\partial x_k} \right\rangle, \tag{3.4}$$

$$B = -\frac{1}{Fr^2} \langle \rho' u_3' \rangle, \quad T_i = \frac{1}{2} \langle u_i' u_j' u_j' \rangle + u_i' p' - \frac{2}{Re} \langle u_j' s_{ij}' \rangle. \tag{3.5}$$

The energy contribution radiated to the background due to the internal wave flux is given by

$$T_p = \int_C \langle p' u_n' \rangle \, \mathrm{d}C, \tag{3.6}$$

where C denotes the closed curve corresponding to the x_2–x_3 boundary and u_n' is the velocity fluctuation in the direction normal to the boundary.

4. Varying the amount of excess momentum

4.1. *Characteristic scales*

From inspection of the mean profiles in figure 3(*a*) one can observe that as the amount of excess momentum increases, the defect velocity, mean kinetic energy, and mean shear all increase. Despite initial differences, in each of the cases considered in this study, the defect velocity follows qualitatively similar behaviour as shown in figure 4(*a*) for the cases with $r_M = 0.25$. In figure 4(*a*) the universal wake evolution for a towed wake proposed by Spedding (1997) is shown as well. The early-time decay of the present study is significantly faster than the $-2/3$ decay rate for a towed wake and the $-4/5$ decay rate for a self-propelled wake in an unstratified fluid as predicted by Tennekes & Lumley (1972), with the decay rate increasing with increasing amounts of excess momentum. The decay rate in the NEQ regime, $20 < t < 150$, is faster than that predicted using Spedding's proposed model although the observed decay exponent of -0.4 matches the value observed by Meunier & Spedding (2006) for a momentumless stratified wake at intermediate time. At late time the defect velocity decayed at a rate comparable to Spedding's universal model, -0.75, and the value predicted for a self-similar momentumless wake in an unstratified fluid, $-4/5$; note also that the same late-time decay was obtained in the unstratified analogue to the present cases given in de Stadler & Sarkar (2011*a*). Differences between cases are reduced when normalized by the initial value of the defect velocity but the data do not completely collapse as shown in figure 4(*b*).

As shown in figure 5(*a*), the MKE is a good surrogate for the defect velocity and has the advantage of being an integrated quantity and therefore showing smoother behaviour than the defect velocity. Both the defect velocity and MKE show a distinct three-dimensional regime at early time where the defect velocity rapidly decays. The three-dimensional regime is followed by a region showing an accelerated collapse (AC) and a region with constant scaling, the NEQ regime, from $20 < t <\approx 150$. At late time, $t > 300$, the scaling changes as the wake enters the Q2D regime. Unlike the defect velocity, the mean kinetic energy for cases with excess momentum collapses when scaled by the initial amount of mean kinetic energy for the $r_M = 0.25$ cases as shown in figure 5(*b*). Differences are present in the near wake and AC region but for $t > 20$ the agreement is excellent with the exception of the $M40r25$ case for $t > 300$. The variation among the $r_M = 0.5$ cases (not shown here) decreases substantially after normalization but the excellent collapse seen in the $r_M = 0.25$ cases is not seen. For

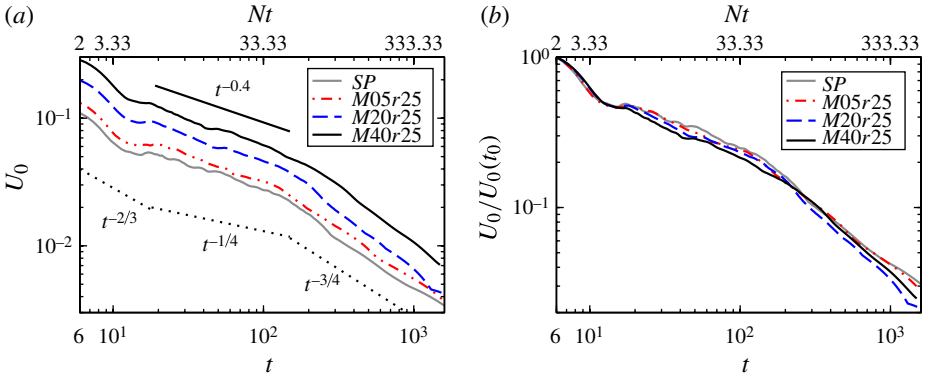

FIGURE 4. (Colour online) (*a*) Defect velocity. The universal wake evolution for a towed wake proposed by Spedding (1997) is shown as a dotted line below the curves. (*b*) Defect velocity normalized by initial value.

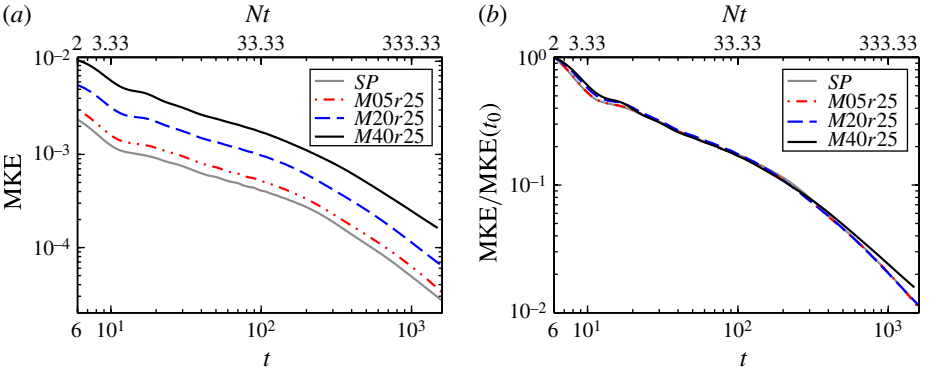

FIGURE 5. (Colour online) (*a*) Integrated mean kinetic energy. (*b*) Integrated mean kinetic energy normalized by initial value.

the unstratified cases in de Stadler & Sarkar (2011*a*), the MKE for the $r_M = 0.25$ cases with excess momentum departed from self-propelled behaviour at intermediate time, $30 < t < 50$ with departure occurring earlier for larger amounts of excess momentum. In the present study, departure can only be observed in the $M40r25$ case and at significantly later time, $t \approx 300$ in the present study versus $t = 30$ for the unstratified case.

Unlike the MKE, the wake dimensions do not collapse when scaled by their initial values. However, scaling by the initial values allows comparison of the relative expansion of the wake in the horizontal and vertical directions for the different cases. As shown in figure 6, the wake width grows larger with increasing amounts of excess momentum. After early differences due to the accelerated collapse, all cases evolve close to $t^{1/3}$, a value which has been observed in both stratified and unstratified towed wake studies and corresponds to the self-similar expansion rate of an unstratified towed wake. Here we note that in the NEQ regime, the cases with increased excess momentum have a slightly larger expansion rate with the $M40r25$ case growing at a rate of 0.42 compared to the 0.30 rate of the *SP* case. At late time, $t > 200$, the expansion rate increases to a value closer to $1/2$. Again the cases

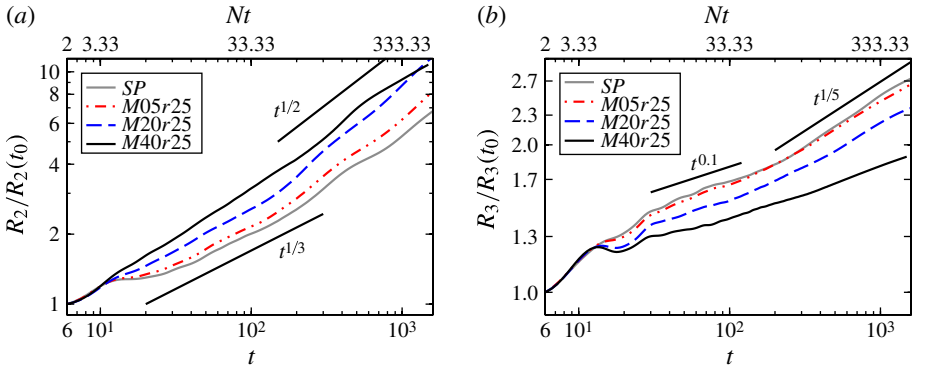

FIGURE 6. (Colour online) Wake dimensions based on mean velocity: (*a*) wake width; (*b*) wake height.

with increased amounts of excess momentum expand faster than the self-propelled case; in the $M40r25$ case the expansion rate is slower than observed for the $M20r25$ case, a result not observed when $r_M = 0.5$. The expansion rate of the wake width is comparable to what was observed in Brucker & Sarkar (2010) and Lin & Pao (1979) and larger than the value of 0.18 observed by Meunier & Spedding (2006).

The wake height shows reduced vertical growth with larger excess momentum. As shown in figure 6, higher values of $R_2/R_2(t_0)$ for the wake are accompanied by lower values of $R_3/R_3(t_0)$ due to momentum conservation. A vertical collapse, shown by the reduction in $R_3/R_3(t_0)$ from $t = 15$ to $t = 20$, is observed in cases with 20 % and 40 % momentum in contrast to the behaviour of the self-propelled wake. The plateau in wake height observed in Lin & Pao (1979) and Brucker & Sarkar (2010) was not observed in the present study and it should be noted that the vertical growth rate at intermediate time is reduced in the present study: 0.10 versus 0.25 in Lin & Pao (1979) and 0.2 in Brucker & Sarkar (2010). The different behaviour in the present study is attributed to low-Reynolds-number effects: the present simulations are conducted at $Re = 10\,000$, which is 3–5 times smaller than that of Lin & Pao (1979) and 5 times smaller than Brucker & Sarkar (2010). In self-propelled wake simulations at $Re = 25\,000$, de Stadler & Sarkar (2011*b*) observed an increased initial growth rate of the wake height and more of a plateau at intermediate time. We note that the reduced wake height with excess momentum would be expected based on intermediate behaviour between the two limiting cases of a self-propelled wake and a towed wake in Brucker & Sarkar (2010).

The wake width and height based on the kinetic energy evolves differently than corresponding quantities based on the mean velocity as shown in figure 7. The wake width based on kinetic energy shows an initial growth until $t = 150$, a contraction from $150 < t < 400$, and growth for $t > 400$. At late time, the value of R_{E2} appears to increase with additional amounts of excess momentum although the $M20r25$ case increases faster than the $M40r25$ case. The wake height based on kinetic energy increased until $t = 150$ and then decreased until $t \approx 800$ when it began to level out. The late-time value of R_{E3} is reduced with increasing amounts of excess momentum.

The contraction in the horizontal, a direction that is not restrained by gravity, occurs only in $R_{E2}(t)$, not in $R_2(t)$. This surprising behaviour can be explained as follows. After an initial expansion due to turbulent diffusion, the wake begins to feel the effect of buoyancy and begins to contract in the vertical. The wake collapse results

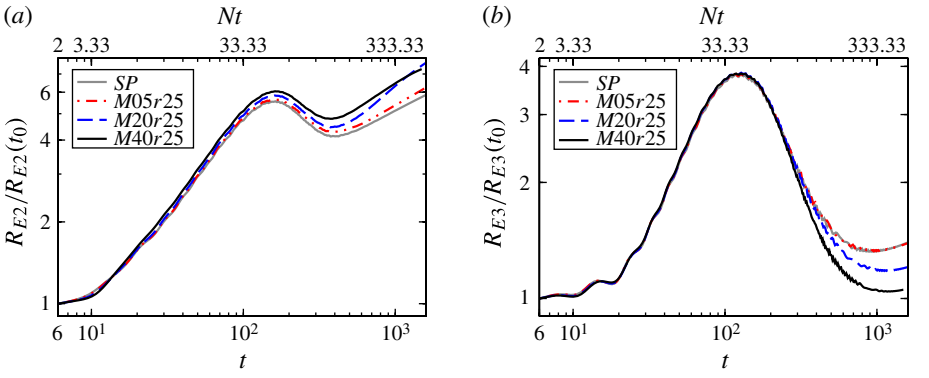

FIGURE 7. (Colour online) Wake dimensions based on kinetic energy: (*a*) wake width; (*b*) wake height.

in the generation of internal waves which carry energy away from the wake into the background. In the NEQ regime, R_{E2} and R_{E3} (see definitions in (3.1) and following text) come to be dominated by the distribution of the turbulent kinetic energy. For R_{E2}, turbulent transport and internal wave radiation result in delayed decrease of turbulent kinetic energy at the horizontal boundary of the wake which results in the numerator of R_{E2} increasing during times when the internal wave radiation is significant and a subsequent decline of the numerator of R_{E2} when the wave flux is reduced. Once the wave flux becomes negligible, $t > 400$, the numerator of R_{E2} becomes approximately constant in time while the denominator, the MKE, continually decreases. For R_{E3}, buoyancy limits the vertical expansion of K so that the majority of the turbulent kinetic energy is confined close to the centreline. The kinetic energy of the outgoing internal waves as they travel out of the domain, amplified by the moment arm $(x_3 - x_3^c)^2$, is the reason for the increase of R_{E3} from $20 < t < 150$. As the internal waves propagate out of the domain R_{E3} decreases, $150 < t < 400$, until R_{E3} becomes dominated by K close to the centreline.

4.2. *Energetics*

As the amount of excess momentum in the wake is increased, the shear in the velocity profile is increased which results in larger production, which leads to larger amounts of energy being extracted from the mean velocity to turbulent fluctuations resulting in increased values of the turbulent kinetic energy and subsequently increased dissipation. This was observed to occur as shown in figure 8. Note that the initial levels of dissipation and production differ due to differences in the velocity fields at the end of the initial adjustment period. The production is initially balanced between the $P_{12} = \langle u_1' u_2' \rangle \partial \langle u_1 \rangle / \partial x_2$ and $P_{13} = \langle u_1' u_3' \rangle \partial \langle u_1 \rangle / \partial x_3$ components. P_{12} remains strictly positive and is in general the dominant term for the production throughout the flow evolution. The value of P_{13} decreases as the effects of stratification begin to be felt and becomes negative during the accelerated collapse, remaining negative throughout the flow evolution with a magnitude of 20 % or less of P_{12} after $t = 40$ which indicates that stratification causes a transfer from turbulent kinetic energy to mean kinetic energy in the vertical direction in the NEQ and Q2D regimes, a result not observed in the unstratified wake. Production is the main sink of mean kinetic energy and removes greater than 80 % of the initial MKE. The collapse of the mean kinetic energy when normalized by the initial value, figure 5(*b*), can be explained by the collapse of the

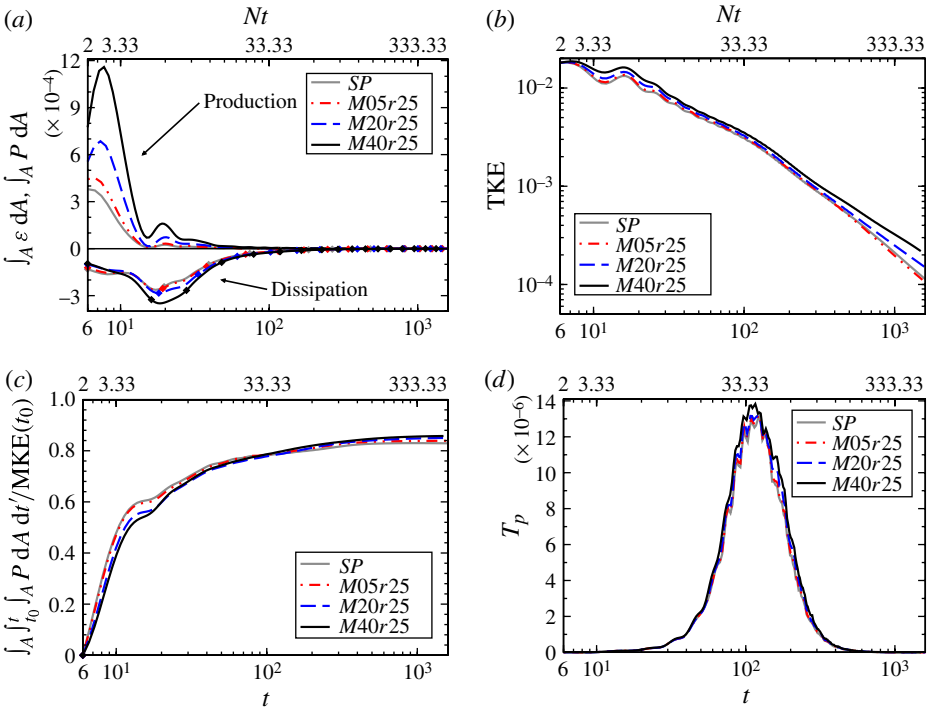

FIGURE 8. (Colour online) Effect of excess momentum on turbulent quantities: (*a*) integrated production and dissipation; (*b*) integrated turbulent kinetic energy; (*c*) cumulative integral of production normalized by initial MKE; (*d*) internal wave flux.

cumulative integral of production for $t > 20$. Higher values of scalar dissipation in the density field (not shown) and slightly reduced values of positive buoyancy flux (not shown) were observed as the amount of excess momentum was increased.

Figure 8(*b*) shows that the difference in TKE between cases increases in the NW region, $10 < t < 15$, and then progressively erodes over time. As the wake begins to feel the effects of stratification, the differences decay at the highest rate, from $16 < t < 26$, and then the decay rate of the differences between the self-propelled and excess momentum cases slows in the NEQ. The additional turbulence generated by production in the NW regime has a smaller value of characteristic time scale, K/ε, when the amount of excess momentum increases which results in the 'new' shear-generated turbulence dissipating faster in the higher excess momentum cases than the turbulence in the self-propelled case.

While quantitative differences are most pronounced at early time, they persist for the duration of the simulation. Despite the relatively large quantitative differences between the *r*25 cases, the qualitative behaviour was similar for the TKE, production, and dissipation. It is interesting to note that the internal wave flux (figure 8*d*) was not as sensitive to excess momentum as the other turbulent quantities.

The partition of kinetic energy between turbulent kinetic energy and mean kinetic energy modes at late time in a self-propelled wake is dominated by the turbulent kinetic energy as observed experimentally by Meunier & Spedding (2006) and numerically by Brucker & Sarkar (2010). Adding excess momentum changes the partition of kinetic energy with larger amounts of excess momentum leading to a more

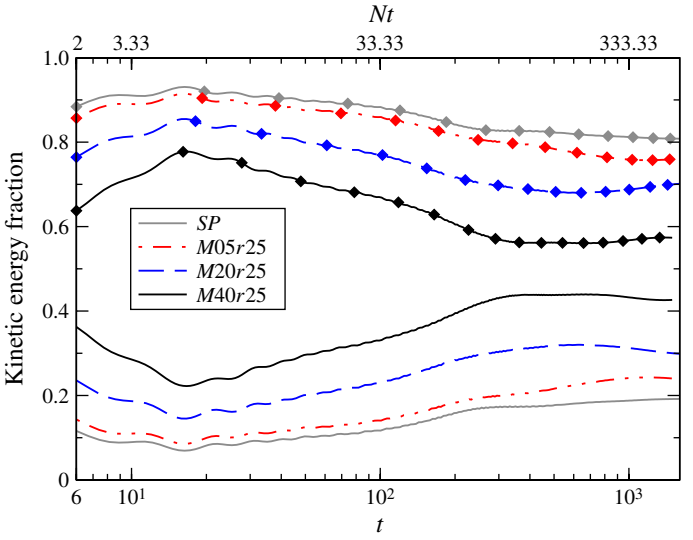

FIGURE 9. (Colour online) Partition of kinetic energy into mean and turbulent modes. Lines without diamonds show MKE and lines with diamonds show TKE.

equipartioned balance of kinetic energy as shown in figure 9. The redistribution of kinetic energy with excess momentum shows that the MKE associated with excess momentum is significantly higher at late time relative to a self-propelled wake. The evolution of TKE/E and MKE/E is similar between cases as can be expected by the qualitatively similar evolutions of TKE and MKE. It is interesting to note that the three flow regimes can be observed in this plot with a region showing decrease of MKE relative to TKE at early time (NW), a region showing decrease of TKE relative to MKE at intermediate time (NEQ), and a region showing a quasi-balance between MKE and TKE at late time (Q2D).

5. Varying the shape of excess momentum

Similar to increasing the amount of excess momentum, reducing the radial extent of the excess momentum increases the defect velocity, mean kinetic energy and shear in the velocity gradient. Note that the $r_M = 0.25$ cases do not disturb the drag lobes whereas the $r_M = 0.5$ cases weaken the velocity in the drag lobes. The largest differences from the *SP* case were observed in the cases with 40 % excess momentum; identical qualitative behaviour with smaller quantitative differences was found in the 20 % and 5 % cases.

The defect velocity in figure 10(a) and mean kinetic energy (not shown) begin at lower values in the $r_M = 0.5$ case than the $r_M = 0.25$ case. The MKE remains lower for the duration of the simulation but the defect velocity becomes almost equal for $t > 700$. While the wake follows the same general trends in evolution with different shapes, NW regime to NEQ regime to Q2D regime, the decay rates in the NEQ and Q2D regimes are different. The wake is larger in the horizontal direction, figure 10(b), and vertical direction (not shown) in the $r_M = 0.25$ case. Since momentum is conserved in the wake, the faster decay of the mean velocity in the $r_M = 0.25$ cases compared to the $r_M = 0.5$ cases leads to larger wake dimensions for

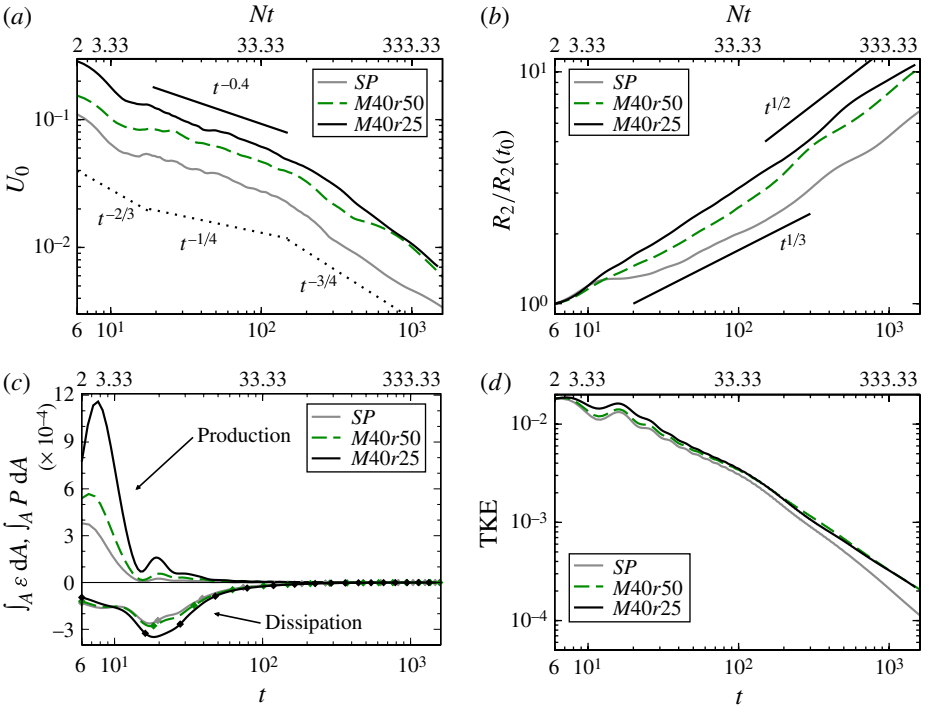

FIGURE 10. (Colour online) Effect of varying the shape of excess momentum: (*a*) defect velocity; (*b*) wake width; (*c*) integrated production and dissipation; (*d*) integrated turbulent kinetic energy.

the $r_M = 0.25$ cases. The same result for the wake dimensions was found to occur in R_{E2} and R_{E3}.

The integrated production, TKE, and dissipation are larger in the $M40r25$ case at early to intermediate time yet the quantitative differences become reduced or disappear at late time as shown in figure 10(*c*,*d*). Similar to the case of increased amount of excess momentum, the increased shear at early time in the $M40r25$ case generates turbulence which increases the TKE; however, the turbulent dissipation rate also increases which reduces the differences between the $M40r25$ and $M40r50$ cases until the TKE in both is comparable when $t > 100$. The wave flux (not shown) shows a small increase in the $M40r25$ case compared to the $M40r50$ case; in the other cases the wave flux shows no difference. In general, differences in statistics with the shape of excess momentum tended to be largest at early time and reduced at intermediate to late time. While quantitative differences do occur in mean and turbulent statistics, the qualitative behaviour of the wake is not sensitive to the shape of the excess momentum for the two cases considered in this study.

6. Wake vorticity

Contour plots of the instantaneous vertical vorticity, ω_3, at the $x_3 = 0$ horizontal plane are used to visualize structures in the wake. As shown in figure 11, at $t = 75$ a vortex street is evident with pairing beginning to occur. The vorticity field appears qualitatively similar to that observed in Voropayev *et al.* (1999) for a steadily moving self-propelled body, their figure 2(*b*), although here we note that Voropayev *et al.*

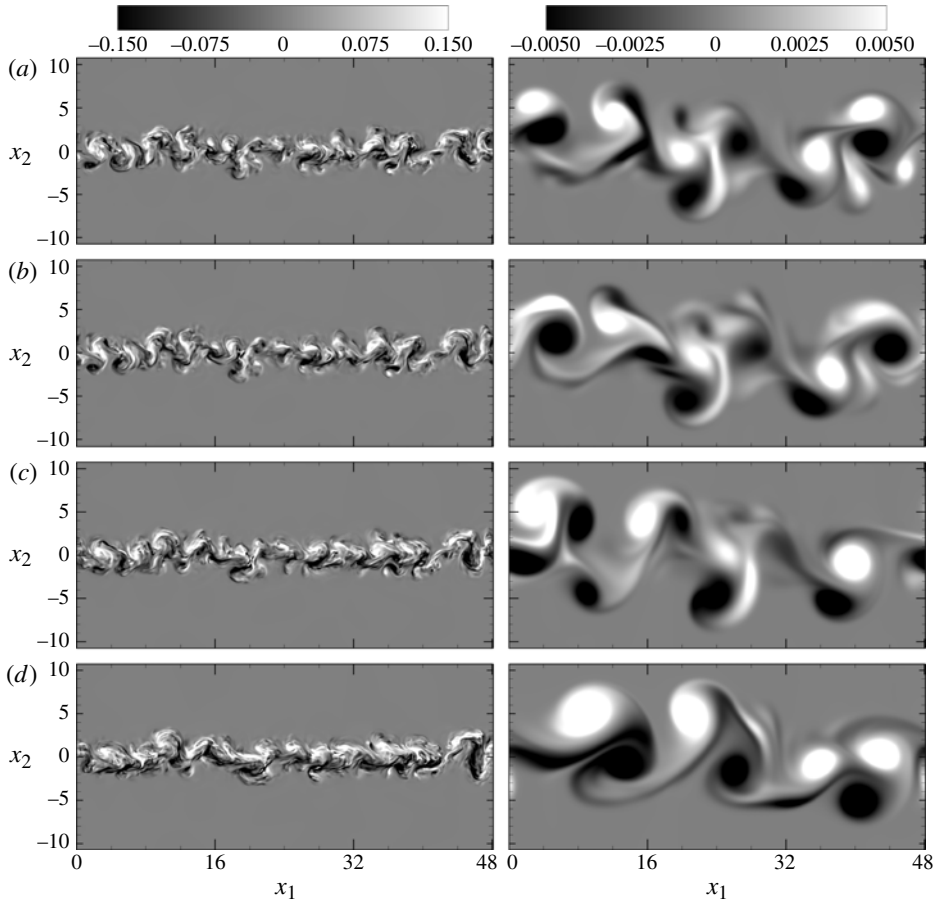

FIGURE 11. $\omega_3(x_3 = 0)$ for the $r_M = 0.25$ cases. Left column: $t = 75$; right column $t = 1400$. (*a*) *SP*; (*b*) *M*05*r*25; (*c*) *M*20*r*25; (*d*) *M*40*r*25.

(1999) report results at significantly lower Reynolds number, $Re \approx 630$, and at $Fr \approx 13$. The number of vortices decreases and their size increases as the amount of excess momentum increases. This effect is more pronounced in the $r_M = 0.25$ cases than the $r_M = 0.5$ cases due to the larger initial vorticity at the centreline of the wake at the start of the simulation. The vorticity fields in the *SP* and *M*05*r*25 cases are extremely similar, small differences occur in the *M*20*r*25 case, and larger differences are evident in the *M*40*r*25 case.

At late time, $t = 1400$, pairing has reduced the number and increased the size of pancake eddies in the wake. Similar to the vorticity field at $t = 75$, small differences from the self-propelled case are present for the *M*05*r*25 and *M*20*r*25 cases. The most significant differences occur in the *M*40*r*25 case. The late-wake pancake eddies in the *SP* and *M*05*r*25 cases are qualitatively similar to the momentumless results of Meunier & Spedding (2006) although the late-wake pancake eddies in the *M*20*r*25 case and especially the *M*40*r*25 case are more reminiscent of the structures behind a towed body as observed in numerical and experimental studies, e.g. Meunier & Spedding (2006), Brucker & Sarkar (2010), de Stadler *et al.* (2010) and Diamessis *et al.* (2011).

The structures observed in all cases are not significantly larger than the structures observed in the case with no excess momentum. This result is in contrast to the results of Voropayev *et al.* (1999) and Voropayev & Fernando (2010) who observed significantly larger dipole structures forming in the late wake when a body manoeuvred in their experiments. One possible reason for the disagreement is that their experiments involved an acceleration performed over a finite time whereas the present study involves a continually acting propulsor generating excess momentum in the wake. In Voropayev *et al.* (1999) and Voropayev & Fernando (2010), a finite amount of momentum is added into the wake which forms a jet-like front region resulting in a region of concentrated strong vorticity that forms several pairs of eddies which pair and merge, often leading to the formation of a single large dipole. The excess momentum wakes considered here occur behind a body moving at constant speed which leads to the formation of a steady system of eddies of comparable size similar to the case of a moving momentum source as discussed in Voropayev & Smirnov (2003). Nevertheless, we note that Voropayev *et al.* (1999) and Voropayev & Fernando (2010) employ a significantly larger initial excess momentum at the beginning of their manoeuvres: the initial thrust to drag ratio in Voropayev *et al.* (1999) is 5, which results in a dipole of significantly larger size than the eddies generated in the present study where the excess momentum is comparatively small. To further test the sensitivity of the size of wake vortices to the initial amount of excess momentum, an additional case (not shown) was run with $r_m = 0.25$ and $c_M = 2.0$ where the size of vortical structures was significantly larger due to the higher initial excess momentum.

7. Wake structure

7.1. *Mean velocity profile*

The mean velocity begins as a doubly inflected profile in both the vertical and horizontal directions. As shown in figure 12(*a*), the horizontal double-inflection is quickly lost and the profile transitions to a Gaussian shape. The mean velocity in the thrust lobe retains a Gaussian shape in the horizontal direction until late time with small disturbances due to coherent structures in the flow, figures 12(*b*) and 13. Meunier & Spedding (2006) also observed a Gaussian profile at the vertical centreplane, $x_3 = 0$, in their propelled-wake experiments when the wake was in the momentum regime; however they did not observe a coherent mean velocity in their momentumless case which is in contrast to the results of the present *SP* case. The drag lobes above and below the thrust lobe transition from an arc structure to a Gaussian structure at late time as shown in figure 13.

In the vertical direction, buoyancy preserves the doubly inflected profile through the far wake as shown in figures 13 and 14. Note that figure 14(*b*) shows data normalized by $x_3/R_{3,x_2=0}(t)$ and $\Delta U_{x_2=0}(t) = (U_{max}(t) - |U_{min}(t)|)|_{x_2=0}$. The data collapsed better at late time by normalizing by the velocity difference in the thrust and drag lobes than by the defect velocity for the *SP* and *M*05 cases, the *M*20 and *M*40 cases collapsed with both normalizations. Although the vertical spread of the wake is weak, the collapse of the data improves when normalized by $R_{3,x_3=0}$. The two velocity scalings become identical in the horizontal direction in the absence of drag lobes and the spread in the horizontal direction necessitates scaling by $R_{2,x_3=0}$ for the data to collapse.

Adding excess momentum changes the relative strength of the thrust and drag lobes but not the qualitative shape of the wake profile in the vertical direction. Figure 15(*a*) shows that the ratio of the velocity magnitude in the thrust lobe to the velocity

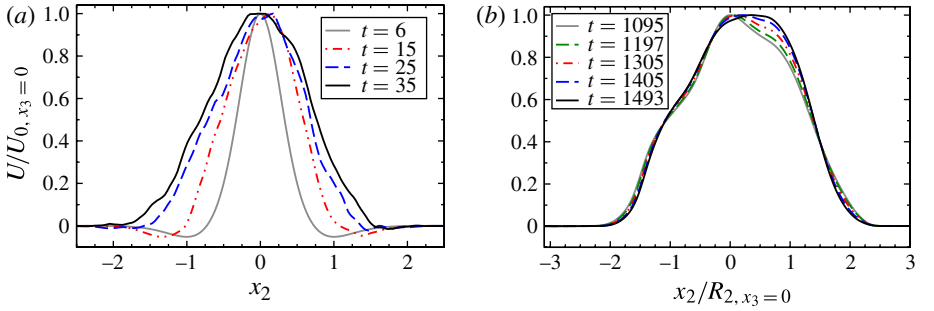

FIGURE 12. (Colour online) Horizontal variation of mean velocity at $x_3 = 0$ for the $M40r25$ case: (*a*) early time; (*b*) late time. The mean velocity is normalized by peak velocity defect $U_0(t)$.

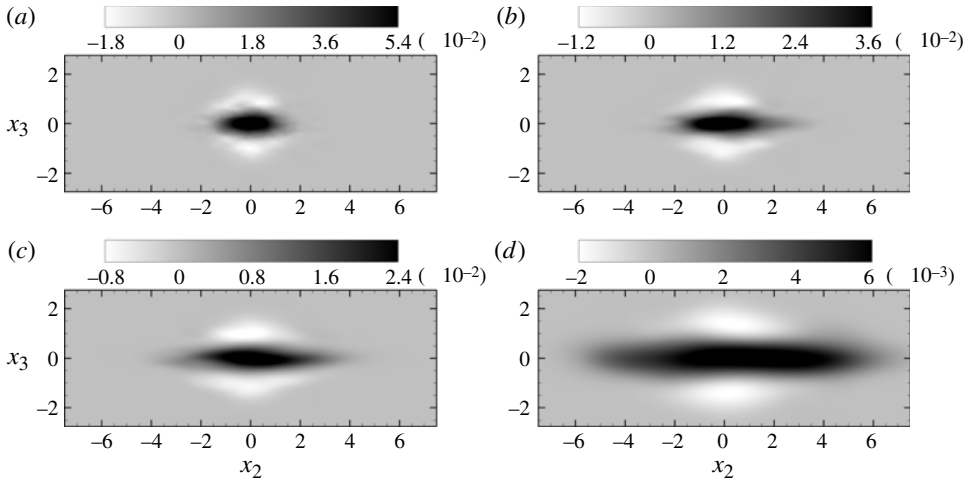

FIGURE 13. Mean velocity evolution for the $M40r25$ case: (*a*) $t = 49$; (*b*) $t = 125$; (*c*) $t = 275$; (*d*) $t = 1405$.

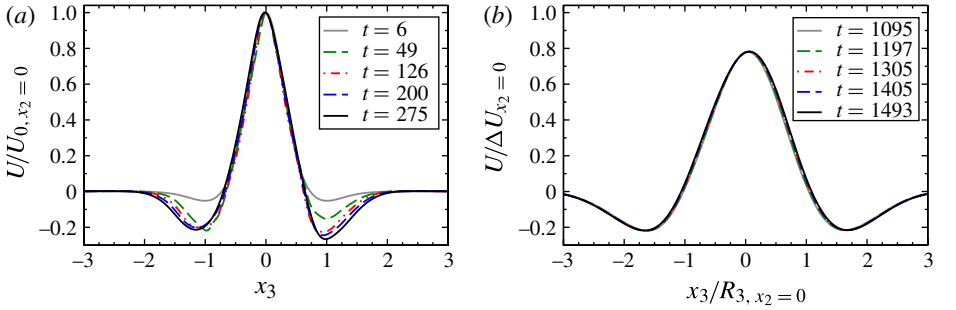

FIGURE 14. (Colour online) Vertical variation of mean velocity at $x_2 = 0$ for the $M40r25$ case: (*a*) intermediate time; (*b*) late time.

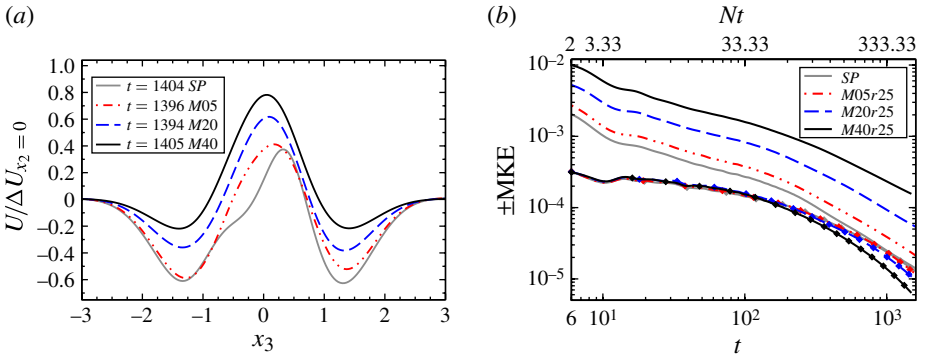

FIGURE 15. (Colour online) (*a*) Effect of increasing excess momentum on the late wake vertical velocity structure. (*b*) Comparison of mean kinetic energy in the thrust and drag lobes. Lines without diamonds correspond to MKE in the thrust lobe and lines with diamonds correspond to MKE in the drag lobes.

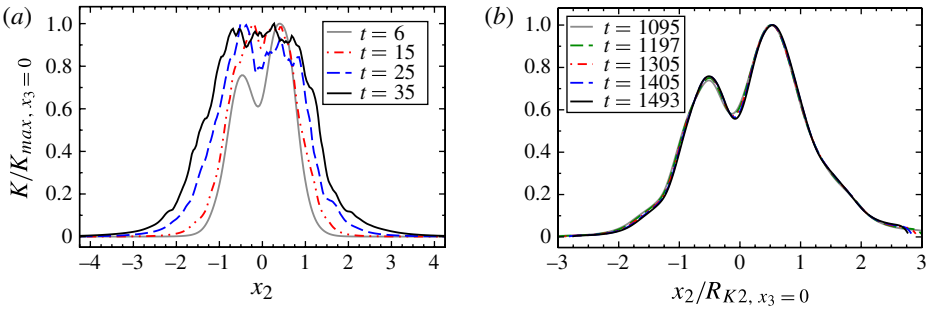

FIGURE 16. (Colour online) Horizontal variation of turbulent kinetic energy at $x_3 = 0$ at early time for the $M40r25$ case: (*a*) early time; (*b*) late time.

magnitude in the drag lobe increases as the amount of excess momentum is increased. The evolution of the velocity in the drag and thrust lobes can be examined by plotting the MKE in the each of the lobes separately. As shown in figure 15(*b*), the MKE in the drag lobes evolves virtually identically at early and intermediate time. At later time, the drag lobes (identified by the mean velocity being negative) decay slightly faster in the presence of excess momentum. The initial value of the MKE in the drag lobe is slightly diminished in the $r50$ cases (not shown) but qualitatively similar behaviour occurs.

7.2. *Turbulent kinetic energy profile*

Just as the wake spreads in the horizontal direction at early time, the turbulent kinetic energy also spreads horizontally with a roughly Gaussian shape, figure 16(*a*). At late time, K in the horizontal direction is dominated by the presence of coherent pancake eddies in the wake, resulting in a doubly humped profile as shown in figures 16(*b*) and 17(*d*). In contrast to K in the horizontal direction, K in the vertical direction does not spread at early time. In the NEQ regime, as shown in figures 17 and 18(*a*), K transitions from an initially Gaussian profile to a compact profile with a sharp central peak in the thrust lobe and small secondary peaks at the outer edges corresponding to the drag lobes. The secondary peaks in K corresponding to the drag lobes are

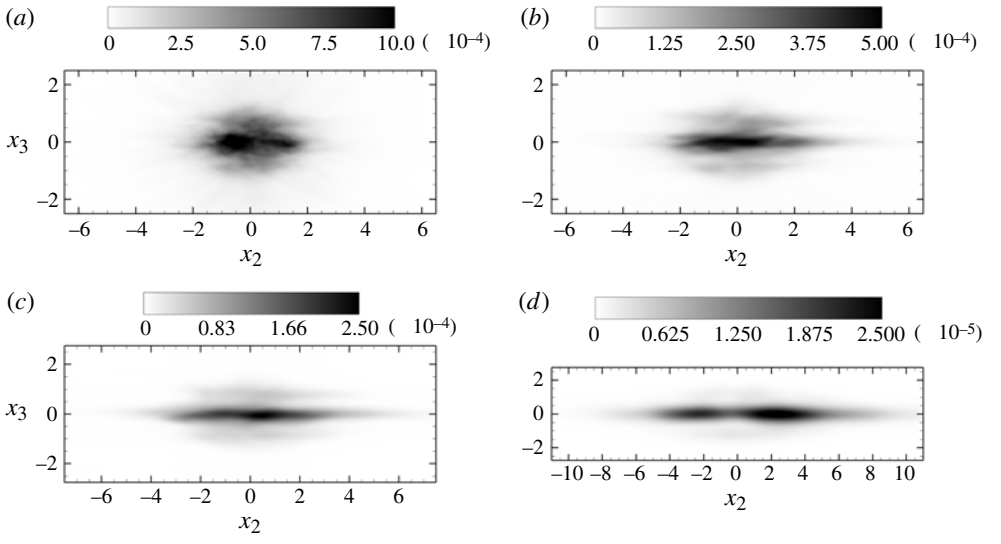

FIGURE 17. Turbulent kinetic energy evolution for the $M40r25$ case: (*a*) $t = 49$; (*b*) $t = 125$; (*c*) $t = 275$; (*d*) $t = 1405$.

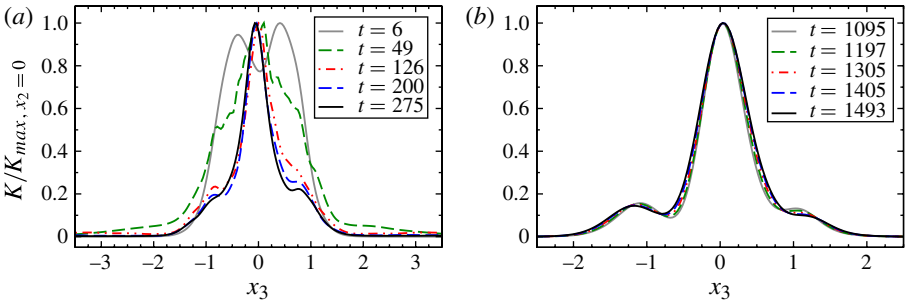

FIGURE 18. (Colour online) Vertical variation of turbulent kinetic energy at $x_2 = 0$ for the $M40r25$ case: (*a*) intermediate time; (*b*) late time.

preserved at late time. As the vertical distribution of K changes very little at late time, it was not necessary to normalize by $R_{K3,x_2=0}$ for the data to collapse. However, one is also able to normalize by $R_{K3,x_2=0}$ and the data remains collapsed. In the horizontal direction K expands continually and it is necessary to scale by $R_{K2,x_3=0}$ to collapse the data.

7.3. *Reynolds stress profiles*

The turbulent viscosity hypothesis states that the Reynolds stress in a given direction is proportional to the velocity gradient in that direction. In the horizontal direction, the Reynolds stress, $\langle u_1' u_2' \rangle$, was found to be proportional to the mean velocity gradient $\partial u_1/\partial x_2$ at all times in the flow evolution (figure 19). This result agrees with Meunier & Spedding (2006) who also observed the validity of the turbulent viscosity hypothesis in the horizontal direction. As shown in figure 20, the turbulent viscosity hypothesis is not valid in the vertical direction as $\langle u_1' u_3' \rangle$ does not appear correlated with the mean velocity gradient. The turbulent viscosity hypothesis was not found to be valid

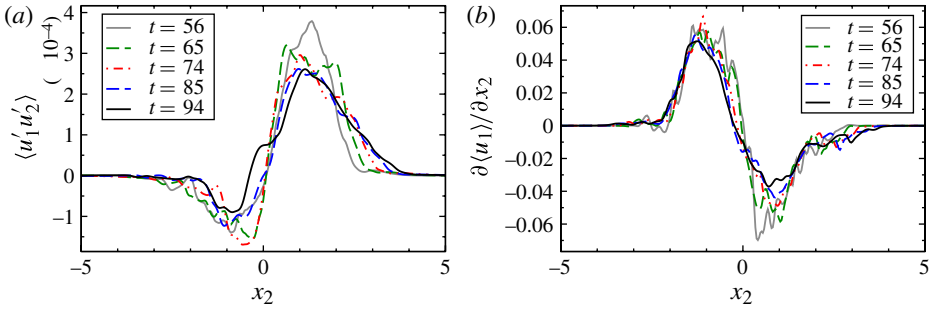

FIGURE 19. (Colour online) Turbulent viscosity hypothesis in the horizontal direction at $x_3 = 0$: (*a*) Reynolds stress $\langle u_1' u_2' \rangle$; (*b*) mean velocity gradient in the horizontal direction.

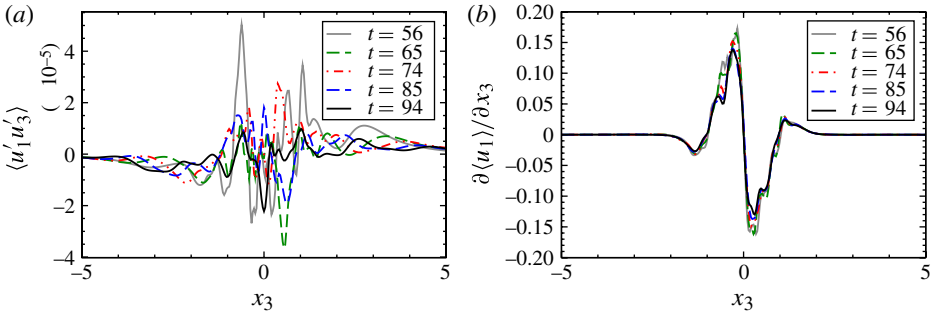

FIGURE 20. (Colour online) Turbulent viscosity hypothesis in the vertical direction at $x_2 = 0$: (*a*) Reynolds stress $\langle u_1' u_3' \rangle$; (*b*) mean velocity gradient in the vertical direction.

at any time for the flow evolution in the vertical direction. The disconnect between the Reynolds stress and the mean velocity gradient in the vertical direction shows that the turbulence in the vertical direction is not classical shear-driven turbulence; recall that the value of the integrated P_{13} component is negative for the majority of the flow evolution. At $x_2 = 0$, $\langle u_1' u_3' \rangle$ fluctuates about zero which is attributable to buoyancy effects and internal wave activity inside the wake core. The fact that the turbulent viscosity hypothesis is not valid is an important result as it is a necessary condition for the momentumless wake predictions of Tennekes & Lumley (1972).

8. Conclusions

Numerical simulations of the effect of excess momentum (up to 40 % excess momentum) on an initially momentumless wake in a stratified fluid have been performed. These simulations are the first usage of DNS for this problem.

We offer the following characterization of what happens to the wake in the presence of a small to moderate acceleration due to an axial jet propulsor. The velocity in the thrust lobe is enhanced owing to excess momentum, leading to an increased defect velocity and mean kinetic energy throughout the evolution. The enhanced velocity gradient leads to increased turbulence production in the horizontal direction and a faster decay of the thrust lobe than the drag lobe. The area-integrated turbulent kinetic energy (TKE) is initially larger owing to enhanced shear production but the dissipation also increases so that, later in the evolution, there is little difference in

TKE between cases. Buoyancy decouples the thrust and drag lobes in the vertical direction, preserving the initial vertical structure and trapping the excess momentum near the vertical centreline. The wake expands in the horizontal direction and large-scale vorticity structures are formed in the late wake.

The wake with excess momentum retains a consistent velocity structure throughout its evolution. The drag lobes in the horizontal direction are quickly lost and the thrust lobe transitions to a Gaussian profile. Similar to the thrust lobe, the drag lobes above and below the thrust lobe transition to Gaussian profiles although at a significantly slower rate than the thrust lobe. In the horizontal direction, the turbulent kinetic energy retains a Gaussian profile with slight disturbances at the top and bottom due to the drag lobes until late time when coherent structures dominate the wake to strengthen the disturbances, leading to a doubly humped profile. Data for the mean velocity were found to collapse at late time when normalized by the peak defect velocity, $U_0(t)$, and the wake width, $R_2(t)$, and the turbulent kinetic energy was found to collapse with $K_{max}(t)$ and $R_{K2}(t)$. The turbulent viscosity hypothesis was found to apply from the near wake to the far wake only in the horizontal direction.

In the vertical direction, buoyancy preserves the initially three-lobed mean velocity structure throughout the evolution of the wake. The turbulent kinetic energy transitions from a Gaussian profile to a sharply peaked single-lobed structure with smaller secondary peaks corresponding to the position of the drag lobes. Data for the mean velocity were found to collapse at late time when normalized by ΔU and $R_3(t)$ and the turbulent kinetic energy was found to collapse with $K_{max}(t)$ and $R_{K3}(t)$. In all cases, there was no clear relationship between the Reynolds stress $\langle u_1' u_3' \rangle$ and the mean velocity gradient in the vertical direction during the evolution of the wake which shows that buoyancy invalidates the turbulent viscosity hypothesis for vertical fluctuation stresses.

A contraction of the horizontal length scale based on kinetic energy in the horizontal direction, R_{E2}, was observed in all cases. This is contrary to usual turbulent diffusion, modelled by local gradient transport, that tends to increase the thickness of turbulent regions. The reason for the contraction is that there is deposition of turbulent kinetic energy into the horizontal wake boundary by non-local transport through internal waves. When that wave flux decreases, the horizontal length scale of the turbulent region decreases. Similarly, the growth and subsequent decay of R_{E3} is also dominated by internal waves although for R_{E3} the internal waves responsible for the expansion and contraction occur outside the wake region whereas for R_{E2} internal waves readjust the turbulence inside the wake region.

The present simulations lead one to conclude that a propelled wake with a small to moderate amount of excess momentum, 40 % or less, behaves qualitatively similar to a self-propelled wake. The qualitatively different behaviour observed by Meunier & Spedding (2006) and suggested by the similarity analysis of Tennekes & Lumley (1972) was not observed. The difference with Meunier & Spedding (2006) could be that their initial mean velocity profiles in the momentumless and excess momentum cases differed qualitatively from those chosen here. For example, they employ a propeller which imparts angular and axial momentum to the wake whereas the present study applies axial momentum using a non-swirling jet. The assumptions underlying the self-similar analysis of Tennekes & Lumley (1972) of constant eddy viscosity and of two independently varying velocity components, a momentumless one and a excess momentum one, are not borne out in the current study. While initial differences are present in the mean kinetic energy and defect velocity, the difference between cases becomes small when velocity and mean kinetic energy are normalized with

the case-dependent initial values. Similarly, early differences in the turbulent kinetic energy, dissipation, and production in the cases with excess momentum compared to the self-propelled case become reduced as the wake evolves.

Acknowledgements

We are pleased to acknowledge the support of ONR grants N00014-07-10133 and N0014-11-10469 administered by Dr R. Joslin. In addition, M.S. received support from an NDSEG Fellowship (HPCMO) and an Achievement Rewards for College Scientists Scholarship (ARCS). Computational resources were provided by the Department of Defense High Performance Computing Modernization Program. All simulations were run on Einstein, a Cray XT5 at the Navy DOD Supercomputing Resource Center (Navy DSRC). We would also like to thank the three anonymous referees whose helpful suggestions improved the quality of this paper.

REFERENCES

ALEKSENKO, N. V. & KOSTOMAKHA, V. A. 1987 Experimental study of an axisymmetric nonimpulsive turbulent jet. *J. Appl. Mech. Tech. Phys.* **28**, 60–64.

BRUCKER, K. A. 2009 Numerical investigation of momentumless wakes in stratified fluids. PhD thesis, University of California San Diego, San Diego, USA.

BRUCKER, K. A. & SARKAR, S. 2010 A comparative study of self-propelled and towed wakes in a stratified fluid. *J. Fluid Mech.* **652**, 373–404.

CHERNYKH, G. G., DEMENKOV, A. G. & KOSTOMAKHA, V. A. 2005 Swirling turbulent wake behind a self-propelled body. *Intl J. Comput. Fluid Dyn.* **19** (5), 399–408.

CHERNYKH, G. G., MOSHKIN, N. P. & FOMINA, A. V. 2009 Dynamics of turbulent wake with small excess momentum in stratified media. *Commun. Nonlinear Sci. Numer. Simul.* **14**, 1307–1323.

CIMBALA, J. M. & PARK, W. J. 1990 An experimental investigation of the turbulent structure in a two-dimensional momentumless wake. *J. Fluid Mech.* **213**, 479–509.

DIAMESSIS, P. J., SPEDDING, G. R. & DOMARADZKI, J. A. 2011 Similarity scaling and vorticity structure in high Reynolds number stably stratified turbulent wakes. *J. Fluid Mech.* **671**, 52–95.

GALLET, S., MEUNIER, P. & SPEDDING, G. R. 2006 Empirical scaling of antisymmetric stratified wakes. *J. Fluids Struct.* **22**, 941–947.

HIGUCHI, H. & KUBOTA, T. 1990 Axisymmetric wakes behind a slender body including zero-momentum configurations. *Phys. Fluids* A **2** (9), 1615–1623.

HYUN, B. S & PATEL, V. C. 1991*a* Measurements in the flow around a marine propeller at the stern of an axisymmetric body. Part 1. Circumferentially-averaged flow. *Exp. Fluids* **11**, 33–44.

HYUN, B. S. & PATEL, V. C. 1991*b* Measurements in the flow around a marine propeller at the stern of an axisymmetric body. Part 2. Phase-averaged flow. *Exp. Fluids* **11**, 105–117.

KOSTOMAKHA, V. & LESNOVA, N. 1995 Turbulent swirling wake behind a sphere with complete or partial drag compensation. *J. Appl. Mech. Tech. Phys.* **36**, 226–233.

LEWELLEN, W. S., TESKE, M. & DONALDSON, C. D. 1974 Application of turbulence model equations to axisymmetric wakes. *AIAA J.* **12** (5), 620–625.

LIN, J. T. & PAO, Y. H. 1979 Wakes in stratified fluids. *Annu. Rev. Fluid Mech.* **11**, 317–338.

MEUNIER, P., DIAMESSIS, P. J. & SPEDDING, G. R. 2006 Self-preservation in stratified momentrum wakes. *Phys. Fluids* **18** (10), 106601.

MEUNIER, P. & SPEDDING, G. R. 2006 Stratified propelled wakes. *J. Fluid Mech.* **552**, 229–256.

NAUDASCHER, E. 1965 Flow in the wake of self-propelled bodies and related sources of turbulence. *J. Fluid Mech.* **22** (4), 625–656.

NOVIKOV, B. 2009 Effect of small total pulse on development of a wake behind the self-propelled bodies. *Thermophys. Aeromech.* **16**, 561–583.

PARK, W. J. & CIMBALA, J. M. 1991 The effect of jet injection geometry on two-dimensional momentumless wakes. *J. Fluid Mech.* **224**, 29–47.

PIQUET, J. 1999 *Turbulent Flows: Models and Physics*. Springer.

POPE, S. B. 2000 *Turbulent Flows*, 1st edn. Cambridge University Press.

ROTTMAN, J. W., DOMMERMUTH, D. G., INNIS, G. E., O'SHEA, T. T. & NOVIKOV, E. 2003 Numerical simulation of wakes in a weakly stratified fluid. *Proceedngs of the 24th Symposium on Naval Hydrodynamics*, pp. 517–533.

SCHETZ, J. A. 1980 *Injection and Mixing in Turbulent Flow*, 1st edn. *Progress in Astronautics and Aeronautics*, vol. 68, American Institute of Aeronautics and Astronautics.

SCHETZ, J. A. & JAKUBOWSKI, A. K. 1975 Experimental studies of the turbulent wake behind self-propelled slender bodies. *AIAA J.* **13** (1), 1568–1575.

SCHOOLEY, A. H. & STEWART, R. W. 1963 Experiments with a self-propelled body submerged in a fluid with a vertical density gradient. *J. Fluid Mech.* **15**, 83–96.

SIRVIENTE, A. I. & PATEL, V. C. 2000*a* Wake of a self-propelled body. Part 1. Momentumless wake. *AIAA J.* **38** (4), 613–619.

SIRVIENTE, A. I. & PATEL, V. C. 2000*b* Wake of a self-propelled body. Part 2. Momentumless wake with swirl. *AIAA J.* **38** (4), 620–627.

SIRVIENTE, A. I. & PATEL, V. C. 2001 Turbulence in wake of a self-propelled body with and without swirl. *AIAA J.* **39** (12), 2411–2414.

SPEDDING, G. 1997 The evolution of initially turbulent bluff-body wakes at high internal Froude number. *J. Fluid Mech.* **337**, 283–301.

DE STADLER, M. B. & SARKAR, S. 2011*a* Simulations of a self-propelled wake with moderate excess momentum in a homogenenous fluid. *Proceedings of the 41st AIAA Fluid Dynamics Conference and Exhibit, Honolulu, Hawaii, June 27–30*. American Institute of Aeronautics and Astronautics.

DE STADLER, M. B. & SARKAR, S. 2011*b* Self-propelled wakes at different Froude numbers in a stratified fluid. *Proceedings of the 7th International Symposium on Turbulence and Shear Flow Phenomena (TSFP-7), Ottawa, Canada, July 28–31*.

DE STADLER, M. B., SARKAR, S. & BRUCKER, K. A. 2010 Effect of the Prandtl number on a stratified turbulent wake. *Phys. Fluids* **22** (9), 095102.

TENNEKES, H. & LUMLEY, J. L. 1972 *A First Course in Turbulence*. The MIT press.

VOROPAYEV, S. I. & FERNANDO, H. J. S. 2010 Wakes of maneuvering body in stratified fluids. In *Progress in Industrial Mathematics at ECMI 2008*, *Mathematics in Industry*, vol. 15, pp. 261–266. Springer.

VOROPAYEV, S. I., FERNANDO, H. J. S., SMIRNOV, S. A. & MORRISON, R. 2007 On surface signatures generated by submerged momentum sources. *Phys. Fluids* **19** (7), 1–10.

VOROPAYEV, S. I., MCEACHERN, G. B., FERNANDO, H. J. S. & BOYER, D. L. 1999 Large vortex structures behind a maneuvering body in stratified fluids. *Phys. Fluids* **11** (6), 1682–1684.

VOROPAYEV, S. I. & SMIRNOV, S. A. 2003 Vortex streets generated by a moving momentum source in a stratified fluid. *Phys. Fluids* **15** (3), 618–624.